National Aeronautics and Space Administration

Extensional terrain formation in icy satellites: Implications for ocean-surface interaction

Author: Samuel Howell (3220)
Robert Pappalardo (3204)

Project Objective

To explore band formation and interaction with interior oceans, we employ fully visco-elasto-plastic 2-D models of faulting and convection with complex, realistic pure ice rheologies. We vary ice shell thickness, fault localization, melting-temperature ice viscosity, and the presence of pre-existing weaknesses. Our results show a spectrum of extensional terrain formation mechanisms that could allow for the surface exposure of frozen ocean material over geologic timescales in ice shells that are thinner, warmer, weakened, and/or convecting.

Background

Europa and Ganymede, Galilean satellites of Jupiter, exhibit geologic activity in their outer H_2O ice shells that might convey material from water oceans within the satellites to their surfaces. Imagery from the Voyager and Galileo spacecraft reveal surfaces rich with tectonic deformation, including long-trend dilational bands on Europa and groove lanes on Ganymede. These features are generally attributed to the extension of a brittle ice lithosphere overlaying a convecting ice asthenosphere. Understanding the formation of extensional terrains and the ability of extensional tectonics to deliver geologically young ocean material that has been frozen in to the ice shell, or "fossil" ocean material, to the surface is critical for understanding the geologic history of icy bodies and predicting where ocean chemistry may be visible on the surface today.

Previous geodynamic models of deformation in icy satellites have primarily focused on convection [e.g. *Mitri and Showman*, 2005], and very few have used a fully formed, non-Newtonian ice rheology [e.g. *Kalousova et al.*, 2016]. Previous studies of ice shell rifting have employed simplified force-balance models [e.g. *Nimmo*, 2004] that fail to capture complex non-Newtonian behavior and the summed effect of viscous, elastic, and plastic deformation.

Terrain Types

Europa: Smooth Bands

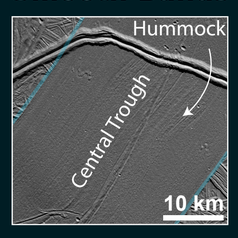

– Band can be removed to reconstruct pre-existing terrain along band margins

Lineated Bands

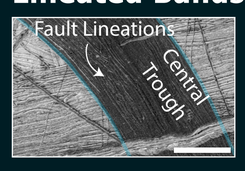

Ridged Bands

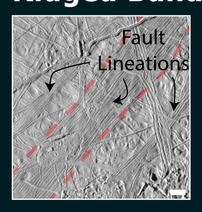

– Terrain reconstruction is not possible by aligning margins

Ganymede: Groove Lanes

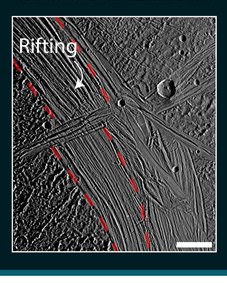

Numerical Modeling Results

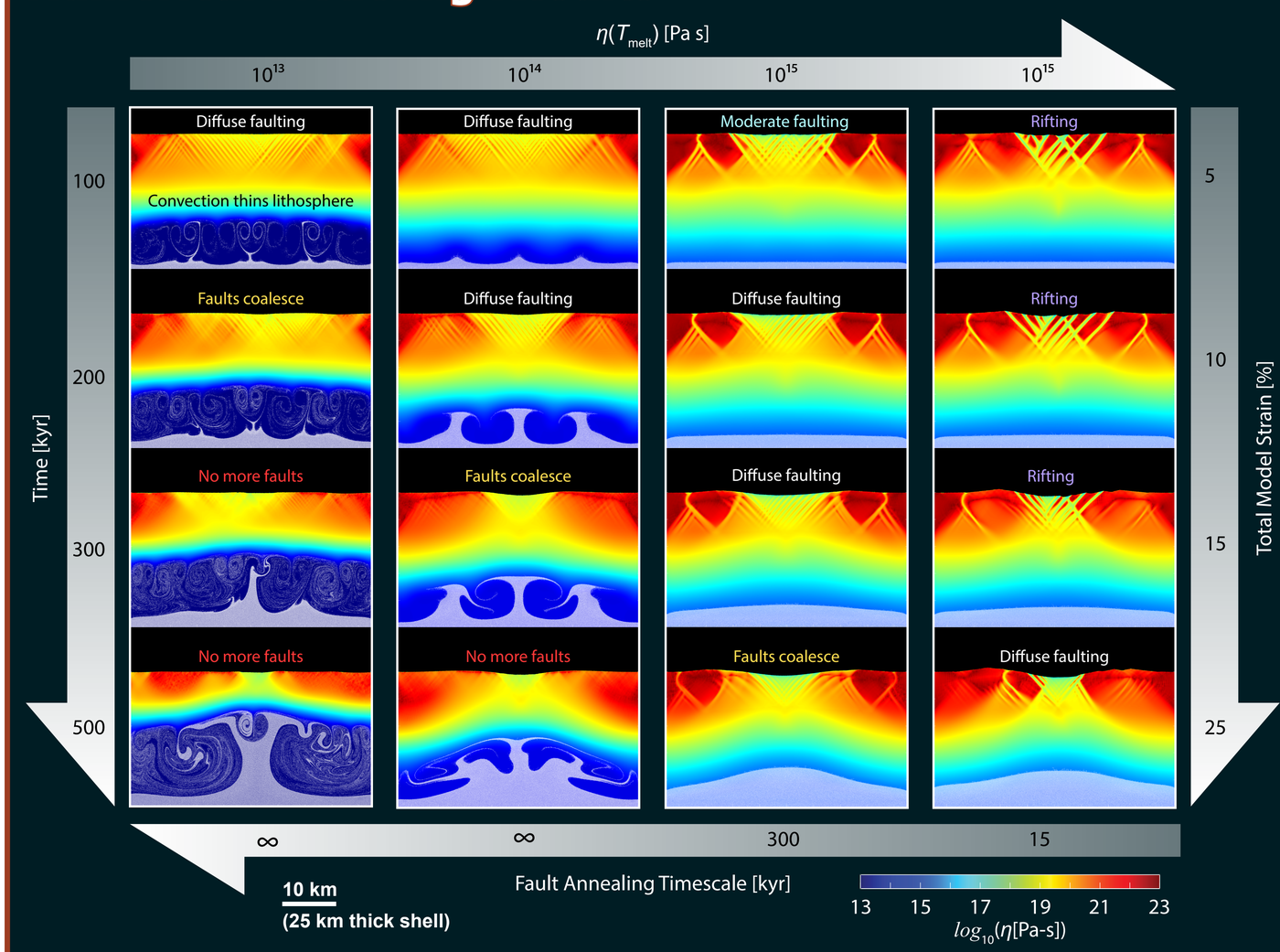

Lithosphere weakened by a thin ice shell, vigorous convection, a lack of fault annealing, or preexisting weaknesses exhibits diffuse faulting that quickly gives way to plastic yielding, producing a smooth or hummocky topography that is symmetrical about a spreading axis; ocean material may be exposed at high strains.

Moderate strength lithosphere produces moderate-scale faulting at low strains, and gives way to plastic yielding at high strains. The initial faulting phase may impact a wide region.

Strong lithosphere results in wide-scale rifting that has an immediate topographic impact over a wide area at low strains with no central axis. Modification of existing terrains would make reconstruction impossible; ocean material is immobile.

Generally, ocean material is unlikely to reach the surface in the absence of convection or in the presence of a very strong lithosphere.

Numerical Approach

We extend the finite-difference software SiStER (Simple Stokes solver with Exotic Rheologies) to simulate two-dimensional (2-D) fully visco-elasto-plastic extensional deformation in an ice shell.

We solve conservation of mass, momentum, and energy in a continuum, and use the particle-in-cell method [*Gerya*, 2010] to rotate stresses, store material properties, and track material provenance.

The ice is treated as a Maxwell material, with a plastic viscosity limited by the Drucker-Prager yield criterion.

The resolution of each model was selected to perform the most efficient simulation where the formation of tectonic features is independent of further refinement. Thus, model resolution varies from 200-300 elements in x and z, with cell resolutions of between 250 and 500 m.

We implement the full composite ductile ice rheology of *Goldsby and Kohlstedt* (2001) to study tectonic deformation and convection in an ice shell to arrive at an effective ductile viscosity, η_v.

$$\eta_v = \left(\frac{1}{\eta_{diff}} + \frac{1}{\eta_{GBS} + \eta_{basl}} + \frac{1}{\eta_{disc}} \right)^{-1}$$

where the averaged viscosities reflect the four deformation mechanisms: grain boundary diffusion (diff), grain boundary sliding-limited basal slip (GBS), basal slip-limited grain boundary sliding (basl), and dislocation creep (disc). Further, the diffusion viscosity at the melting temperature (the minimum model viscosity) is varied between 10^{13} and 10^{15} Pa-s.

Example Model Output

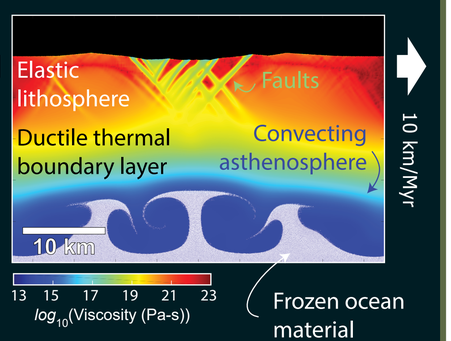

Deformation Mechanisms

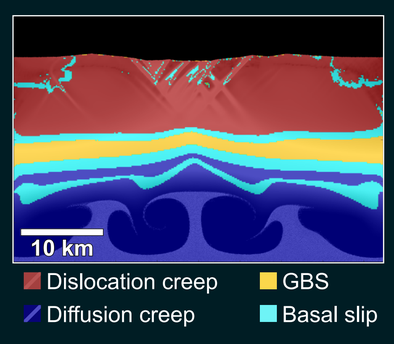

Innovations in ice-tectonics modelling:

- Includes viscous flow, plastic deformation, and elastic bending
- Includes four-component Ice I rheology, with both Newtonian and non-Newtonian deformation mechanisms
- Tracks the movement of ocean ice frozen into the shell

Conclusions

There exists a spectrum of extensional terrains on icy satellites.

Smooth bands on Europa reflect a weaker ice shell that opens plastically and symmetrically.

Groove lanes, and perhaps much of the grooved terrain, on Ganymede represent the other end member, reflecting a strong ice shell that undergoes wide-spread lithospheric rifting, even at low strains.

Lineated bands and ridged bands on Europa are intermediate between these extremes.

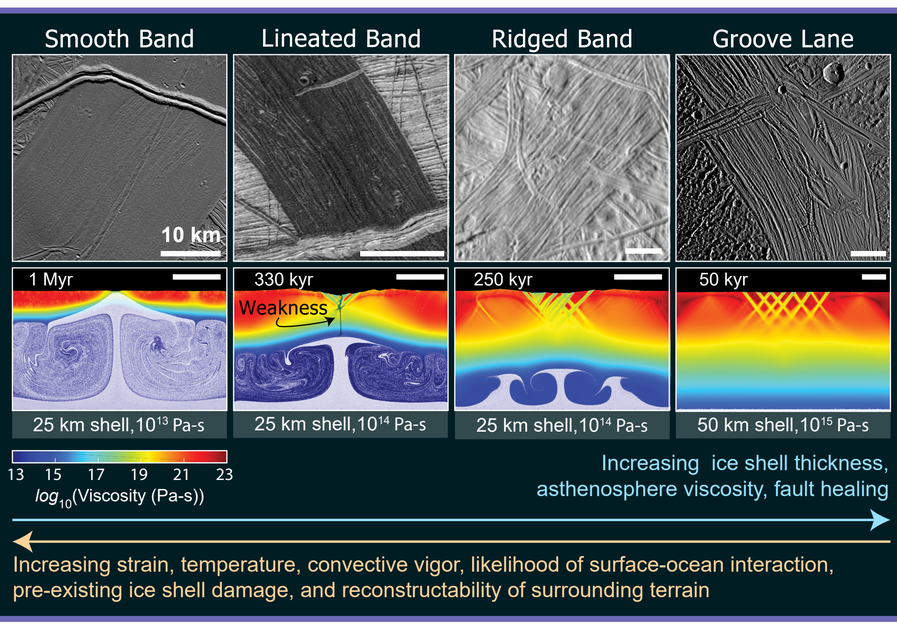

Relevance to proposed and ongoing missions

Understanding how and where frozen ocean material might be exposed may inform targeting and site selection for currently planned and future missions (e.g. Europa Clipper, JUICE, Europa Lander).

These results may impact planetary protection studies, as they demonstrate it is unlikely that extensional terrains on Ganymede will be in contact with the ocean, even on geologic timescales, and that interaction on Europa may only occur during smooth band formation.

Further, these results may have broader implications for extensional feature formation in other icy satellites and small bodies.

National Aeronautics and Space Administration
Jet Propulsion Laboratory
California Institute of Technology
Pasadena, California

www.nasa.gov

Poster No. P-01

National Aeronautics and Space Administration

Detection of outbursts during the summer of 2015 with Rosetta

Adeline Gicquel (3222)
Paul A. Von Allmen (3980)

Introduction – Rosetta mission

The ESA (European Space Agency) Rosetta spacecraft was launched on March 2, 2004 and reached comet 67P/Churyumov-Gerasimenko (67P) in August of 2014. A great deal of data on the nucleus and the coma of the comet were acquired by the instruments onboard Rosetta. The ESA's Rosetta spacecraft had the unique opportunity to follow the activity and morphology of comet 67P during its journey toward the Sun. Close to perihelion in August 2015, a display of outbursts on 67P, known as the summer fireworks (Vincent et al. 2016), was observed with the Optical, Spectroscopic, and Infrared Remote Imaging System (OSIRIS) and the NACVAM. Vincent et al. (2016) reported the detection of 34 outbursts (one every 2.4 nucleus rotations).

An outburst is defined as a bright event having a very short duration with respect to the rotation period of the nucleus. The increase of the brightness of the coma is due to the release of gas and dust (Gicquel et al. 2017). Gicquel et al. (2017) studied a bright outburst, which was observed in the southern hemisphere on July 29, 2015. They have shown that outbursts are in fact a combination of both gas and dust, in which the active surface at the source location of the outburst is believed to be approximately 10 times more active than the average rate found in the surrounding areas.

In the case of the Microwave Instrument for the Rosetta Orbiter (MIRO), the most useful scan pattern for tracking gas abundance before, during, and after an outburst was a series of back-and-forth scans across the nucleus along the comet-Sun line. We identified a spectral feature that is indicative of high velocity gas moving toward the spacecraft as being associated with outbursts. The negative frequency of this feature is due to the Doppler effect.

In this particular study, we will use a Monte Carlo simulation to model the gas distribution in the coma and to add the dust in the future. The model assumes that the gas production becomes only a function of the comet-Sun distance. In the future we will add the dust trajectories. The goal is to understand the mechanisms producing the outburst and the activity.

Observations - Methodology

Data with the OSIRIS Cameras, the NAVCAM and the MIRO instrument

OSIRIS, composed of the wide angle camera (WAC; 230 - 750 nm) and the narrow angle camera (NAC; 250 - 1000 nm), were dedicated to mapping the nucleus of comet 67P and to characterizing the evolution of the comet's gas and dust (Keller et al. 2007). The NAVCAM is a navigation camera.
MIRO is a submillimeter radiometer equipped with two continuum channels at 188 and 562 GHz and a high spectral resolution heterodyne spectrometer working in a frequency-switching mode that targets dedicated H_2O, CH_3OH, CO, and NH_3 lines in the 548–579 GHz range (Gulkis et al. 2007).

Method

Check if the MIRO scan was useful for identifying gas abundances before, during, and after an outburst → (Same pointing) Search for the detection of the $H_2{}^{16}O$ emission line at -1.5 km s^{-1} in the MIRO spectra → ($H_2{}^{16}O$ detection) Examine the illumination conditions at the time of the observations around the source location of an outburst → (Sun illumination) Run the DSMC for water gas and the homogeneous coma to compare with the images

Results – Before the outburst

NAVCAM sequence 2015-08-08

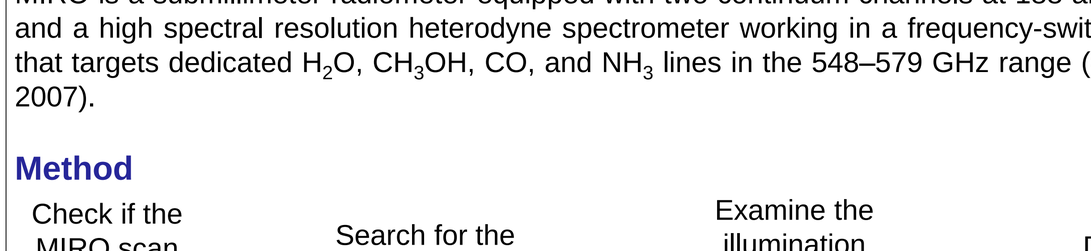

NAVCAM sequence 2015-08-22

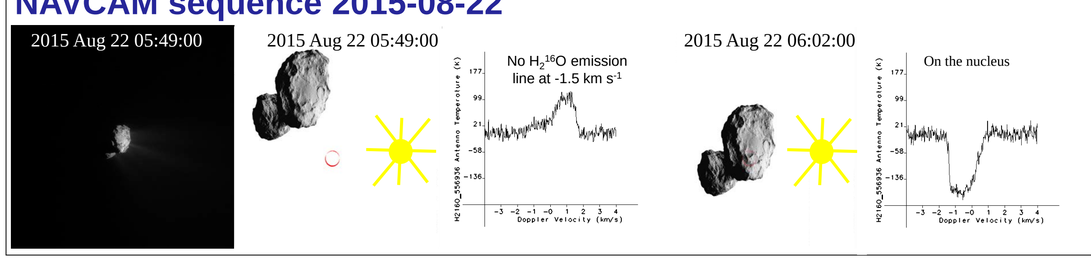

Results – After the outburst

NAVCAM sequence 2015-08-08

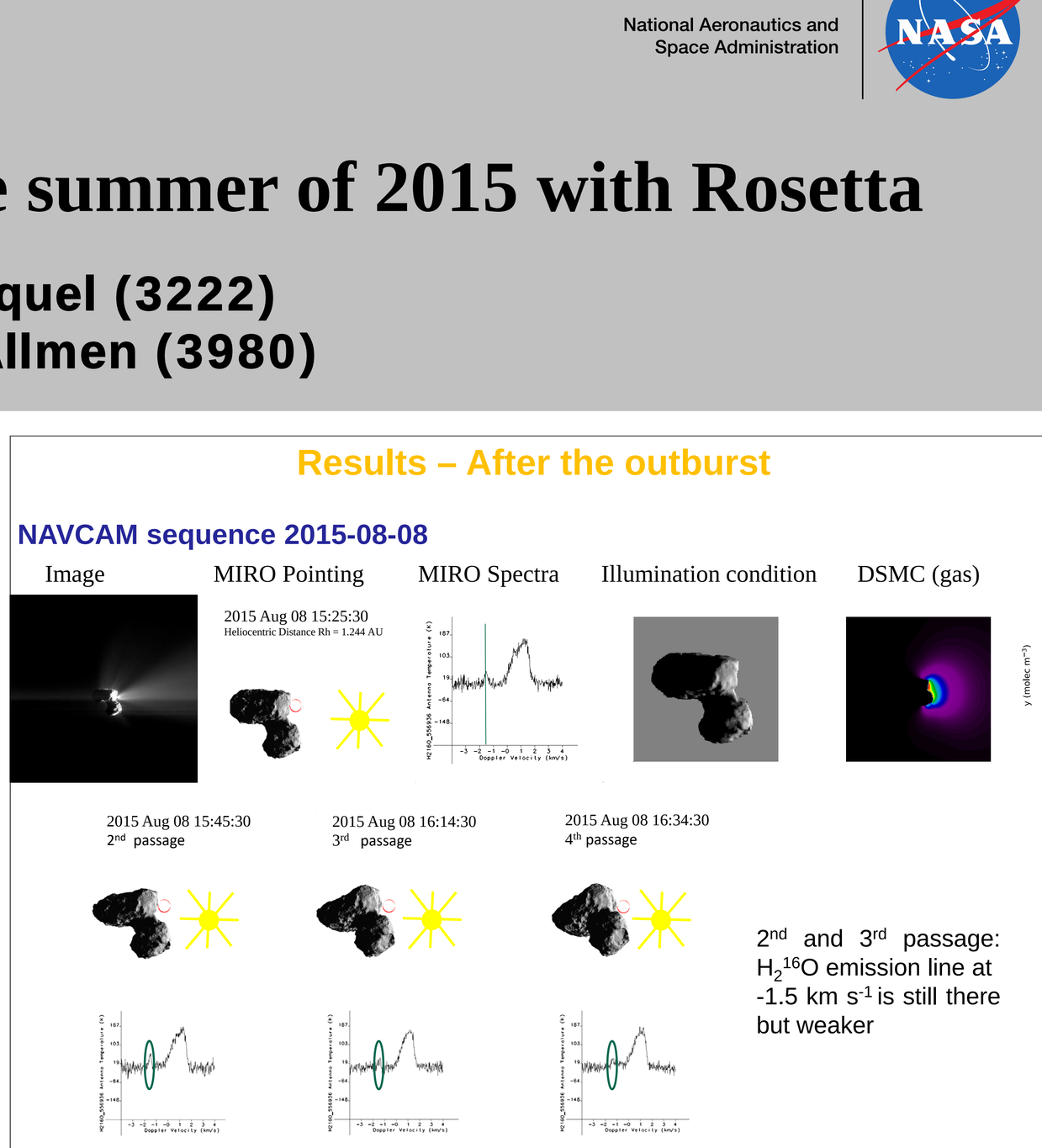

2nd and 3rd passage: $H_2{}^{16}O$ emission line at -1.5 km s^{-1} is still there but weaker

NAVCAM sequence 2015-08-22

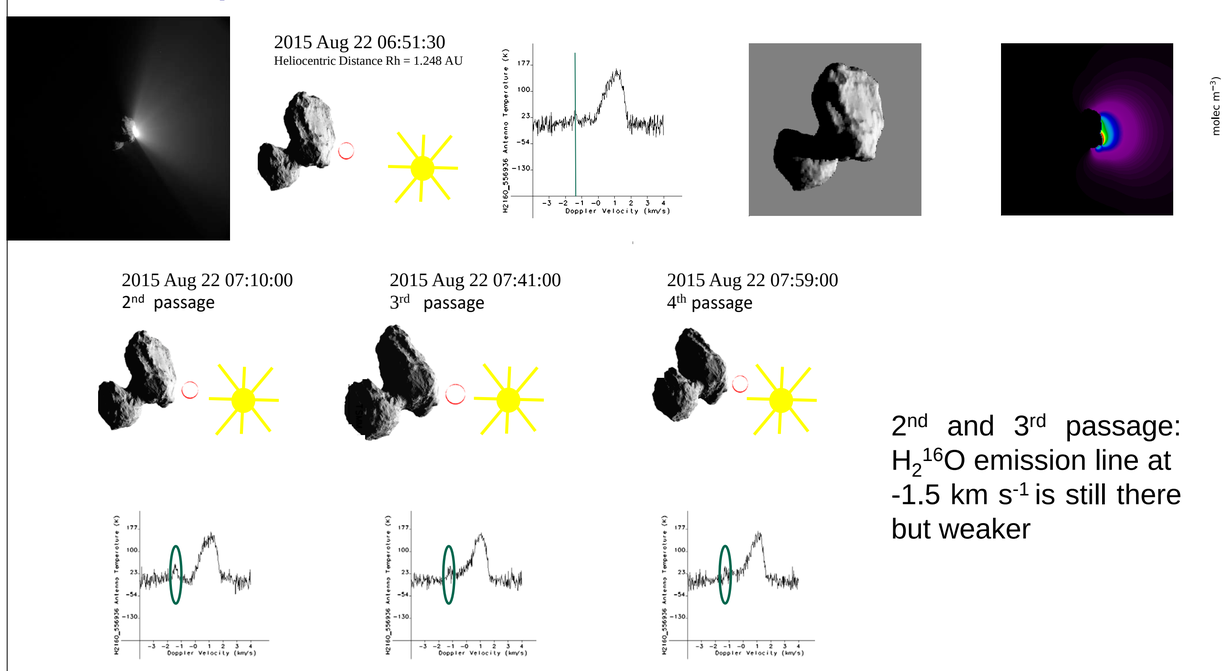

2nd and 3rd passage: $H_2{}^{16}O$ emission line at -1.5 km s^{-1} is still there but weaker

Conclusion and Work in Progress

Comparison OSIRIS/NAVCAM/MIRO Data

- Detection of 6 outbursts with MIRO during summer 2015
- Detection of a high-velocity gas feature for each of the 6 outbursts detected with MIRO
- Detection of 1 outburst not observed with OSIRIS or the NAVCAM
- Activity follows the insolation/illumination

Future work to be done with MIRO

- Calculate the gas production rate form the $H_2{}^{16}O$ emission line

Future work to be done with the DMSN model

- Add the the dust trajectories using three forces acting on the grains: drag force, gravity and radiative pressure
- Create an active surface at the source location of the outburst

We hope to better understand the physics of outbursts and how dust is lifted by gas by comparing model results to OSIRIS images (sensitive to the dust abundance) and MIRO spectra (sensitive to the gas abundance and velocity).

References

Gicquel, A., Rose, M., Vincent, J.-B., et al. 2017, MNRAS, http://arxiv.org/abs/1706.02729
Gulkis, S., Frerking, M., Crovisier, J., et al. 2007, Space Sci. Rev., 128, 561
Keller H. U., Barbieri, C.; Lamy, P., et al., 2007, Space Sci. Rev., 128, 433
Vincent, J.-B., A' Hearn, M. F., Lin, Z.-Y., et al. 2016, MNRAS, 462, 184

National Aeronautics and Space Administration
Jet Propulsion Laboratory
California Institute of Technology
Pasadena, California

www.nasa.gov

Poster No. P-02

Ice sintering timescales at Europa and implications for surface properties

Jamie Molaro (3223), Gareth Meirion-Griffith (374F), Cynthia Phillips* (398H), Robert Pappalardo* (3204). *Postdoctoral Advisors

National Aeronautics and Space Administration

Poster # P 03

Background

Ice sintering is a form of frost metamorphism whereby adjacent grains experience the diffusion of material to their contact region, forming a "neck" between them and densifying over time. Understanding this process is critical to characterizing the microstructural surface properties of icy bodies, which has important implications for the interpretion of remote sensing data. For example, studies of nitrogen ice sintering on Triton have found that non-porous ice slabs can form over seasonal timescales, consistent with telescope observations of absorption features. Other studies have found that sintering on comets can affect their thermal conductivity, and radiation-induced diffusion leads to thermal anomalies observed on Saturnian moons. Additionally, understanding ice sintering timescales on Ocean Worlds improves our ability to model the strength characteristics of icy regoliths, a key metric for future surface exploration efforts. Here we model pressureless (no overburden) sintering of spherical water-ice grains and validate the results with a laboratory experiment. We also model ice at the surface of Europa to obtain a first-order approximation of its sintering timescale and properties.

Model

We implement the numerical model of Swinkels and Ashby (1981) [1], which is most commonly used for this purpose. Modification of spherical, contacting grains is driven by surface, volume, and grain-boundary diffusion mechanisms (Fig 1) that **contribute to either neck growth or densification (decrease in interparticle distance)**, with **d**ifferent mechanisms dominating during different stages:

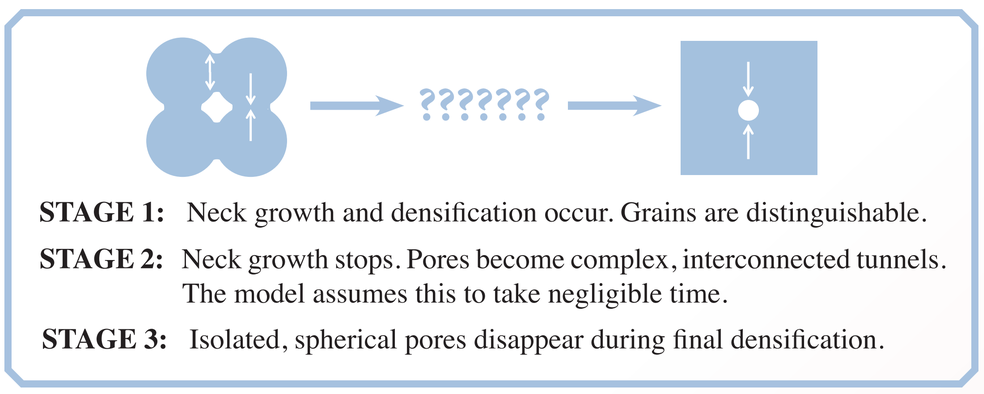

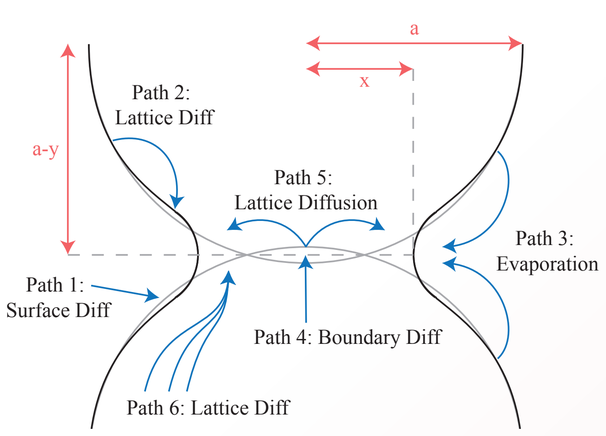

Figure 1. Non-densifying (paths 1-3) and densifying (paths 4-6) diffusion mechanisms. Note that radiation induced diffusion [3] is not yet included in the model, but is not expected to dominate at Europa.

During stage 1, the rates of change of the neck size (x), interparticle distance (y), and density (Δ) are proportional to the sum of the diffusive currents (V):

$$\dot{x} \propto \frac{1}{2\pi x}\sum_{1}^{6}\dot{V} \qquad \dot{y} \propto \frac{1}{\pi x^2}\sum_{4}^{6}\dot{V} \qquad \dot{\Delta} \propto \frac{\dot{y}/a}{(1-y/a)^4}f(\alpha)$$

where a is the original grain radius, and $f(\alpha)$ is a function of the grain packing density. **The key parameters are temperature, and the surface (2.2×10^{-13} to 1.4×10^{-8} m^2/s) and volume (10^{-23} to 1.5×10^{-3} m^2/s) diffusion coefficients**, which are not well constrained for ice. Results are presented in terms of **relative neck size** (neck size/grain diameter), **relative density** (density of aggregate/pure material), and **homogolous temperature** (temperature/melting temperature).

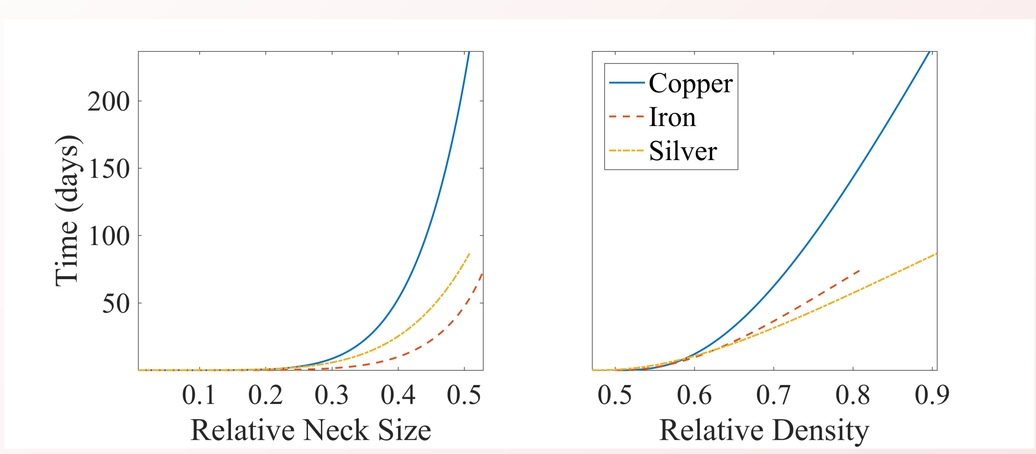

Figure 2. Estimated relative neck size and density throughout stage 1 sintering of 10 μm metal grains, starting at a relative density of 0.47 and a homologous temperature of 0.5. These results are consistent with both the predictions and laboratory data in Swinkels and Ashby (1981) [1]. **Note the density of the metals at the end of stage 1. Stage 3 for these materials (not shown) begins at a relative density of ~0.9, justifying the elimination of stage 2 in the calculation.** Instead, stage 2 is linearly interpolated between the end of stage 1 and beginning of stage 3.

Comparison to Experiment

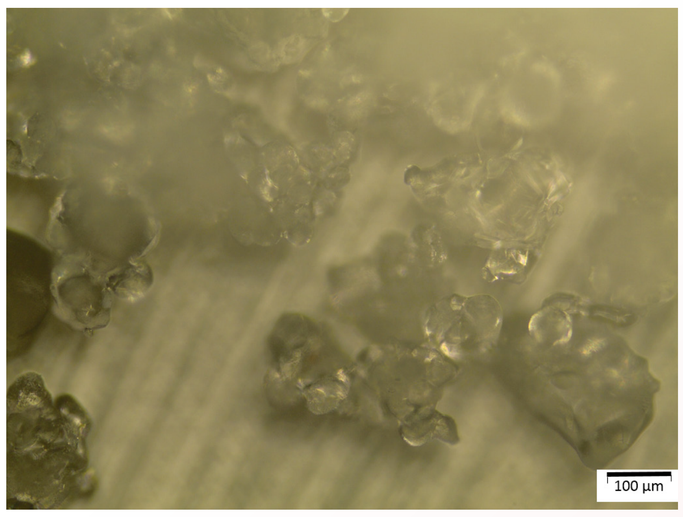

Figure 3. Microscope image of ice grains produced in the laboratory after 9 days stored at -20 C. Spherical, water-ice grains (10-70 μm in diameter) were produced by atomizing distilled water into an LN2 bath. We filled two 60 mm diameter cylinders with 500 ml of ice each, yielding an initial density of 0.45 g/ml. **The cylinders were stored in dehumidified freezers at -20 C and -80 C for 9 days, resulting in an increase in relative density of 3% and 0%, respectively.**

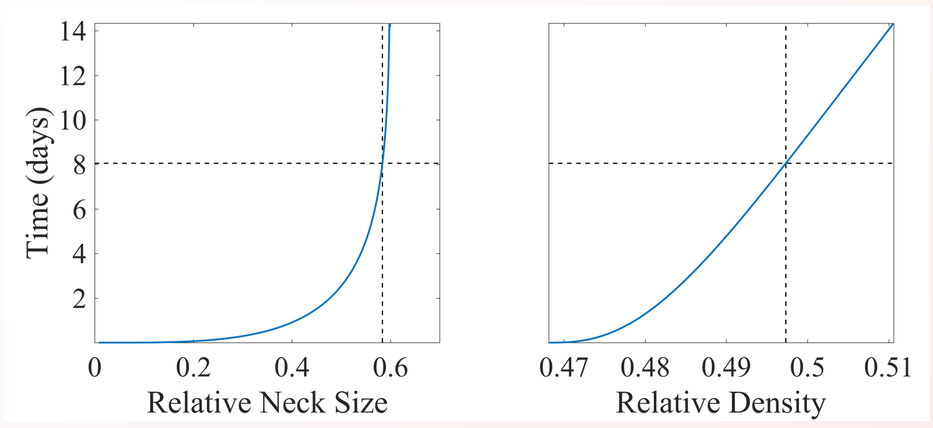

Figure 4. Predicted neck size and density throughout stage 1 for 10 μm ice grains at -20 C. **The model predicts that the increase in relative density observed in our -20 C sample should occur after ~8 days (dotted lines),** and that the end of stage 1 should occur at ~14 days. The predicted density change for the -80 C sample is within measurement uncertainty, and thus also consistent with observations.

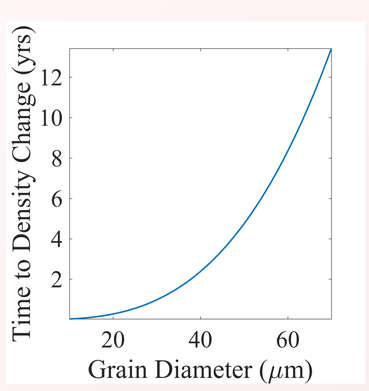

Figure 5. The variation in predicted time to achieve our observed density change demonstrates that **sintering timescales are extremely sensitive to grain size.** Since small grains sinter faster and are more mobile during particle rearrangement, the majority of sintering in our samples occurred in the 10 μm grains. Thus, Figure 4 is a reasonable fit to observations, though future work will explore the role of grain size distribution in detail.

Application to Europa and Conclusions

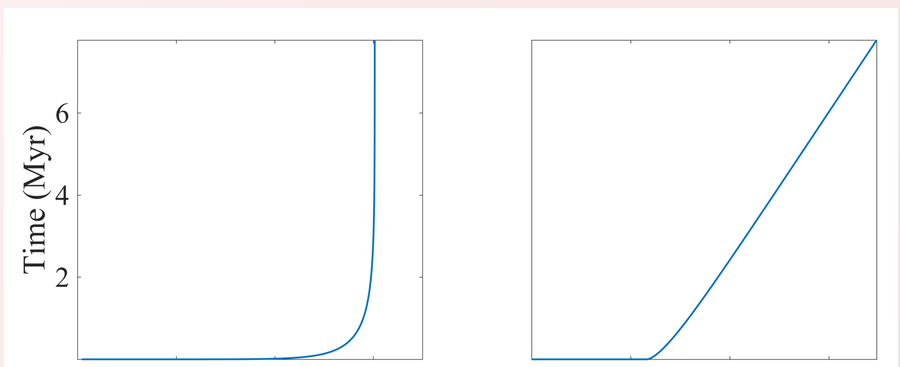

Figure 6. Estimated time for 10 μm ice grains at 136 K to reach the end of stage 1, estimating a **sintering timescale at Europa of ~7.7 Myr** (4.7 - 29.8 Myr). These results predict that ice grains on Europa would experience neck growth, but no substantial densification over its surface age, suggesting that **ice regolith at the surface may form a porous and weak crust.** This has important implications for future exploration efforts, both in the context of interpreting remote sensing data and attempting to land a spacecraft. **Sintering also interacts with other processes, adding to the complexity of characterizing icy surfaces.** For example, sputtering preferentially removes larger grains and may enhance sintering rates and changes in ice porosity will affect the surface response to micrometeorite impacts.

The slow rate of densification relative to neck growth in ice contrasts strongly with the behavior of metals (Fig. 2). Swinkels and Ashby (1981) eliminated stage 2 from the model because neck growth and densification happen on similar timescales in metals, and the density at the end of stage 1 and the beginning of stage 3 are close. However, **this assumption does not apply to ice and thus the model does not accurately quantify densification in these cases**. Previous studies of sintering on icy bodies have used partial-implementations of the model [e.g., 2, 3] that do not reveal this issue, and **may have underestimated these timescales** and/or not fully understood the implications of their results.

[1] Swinkels and Ashby (1981), *Acta Metallurgica 29.2*: 259-281. [2] Eluszkiewicz (1991), *JGR Space Physics 96.S01*: 19217-19229. [3] Schaible et al. (2016), *Icarus*.

National Aeronautics and Space Administration
Jet Propulsion Laboratory
California Institute of Technology
Pasadena, California
www.nasa.gov

Acknowledgement: Part of this work was supported by an appointment to the NASA Postdoctoral Program at the Jet Propulsion Laboratory, California Institute of Technology, under contract with NASA, administered by the Universities Space Research Association through a contract with NASA.

National Aeronautics and Space Administration

The Formation and Evolution of Occator Crater on Ceres

Jennifer E. C. Scully (3223)
Carol A. Raymond (4080)

- INTRODUCTION & METHODS -

- The Dawn spacecraft observed faculae (bright spots) in Ceres' Occator crater.
- The single scattering albedo of Occator's faculae is 0.67-0.80, and of average Ceres is 0.09-0.11 (Li et al., 2016).
- Cerealia Facula is in the center, in a ~9 km wide and ~700 m deep pit, and the Vinalia Faculae are in the eastern crater floor (Nathues et al., 2015; Schenk et al., 2017).
- The faculae are mostly sodium carbonate, which is distinct from Ceres' average surface (De Sanctis et al., 2016).
- The crater is ~20-30 million years old (Nathues et al.; Neesemann et al., 2017).

- Here we present a detailed geologic map of the interior of Occator crater, which is one of the necessary inputs to decipher the geologic history and formation mechanism of Occator and the faculae.

- Our basemap is a 35 m/pixel clear filter mosaic, obtained by Dawn's Framing Camera (Roatsch et al., 2016).
- We also use a shape model with a lateral spacing of ~32 m/pixel and ~1.5 m height accuracy to inform our mapping (Jaumann et al., 2017).
- We performed the mapping in ArcGIS 10.3 and followed USGS mapping guidelines.

- ***I am travelling today and will unfortunately miss the poster session: please email me if you would like to talk about this project (jennifer.e.scully@jpl.nasa.gov).***

- RESULTS -

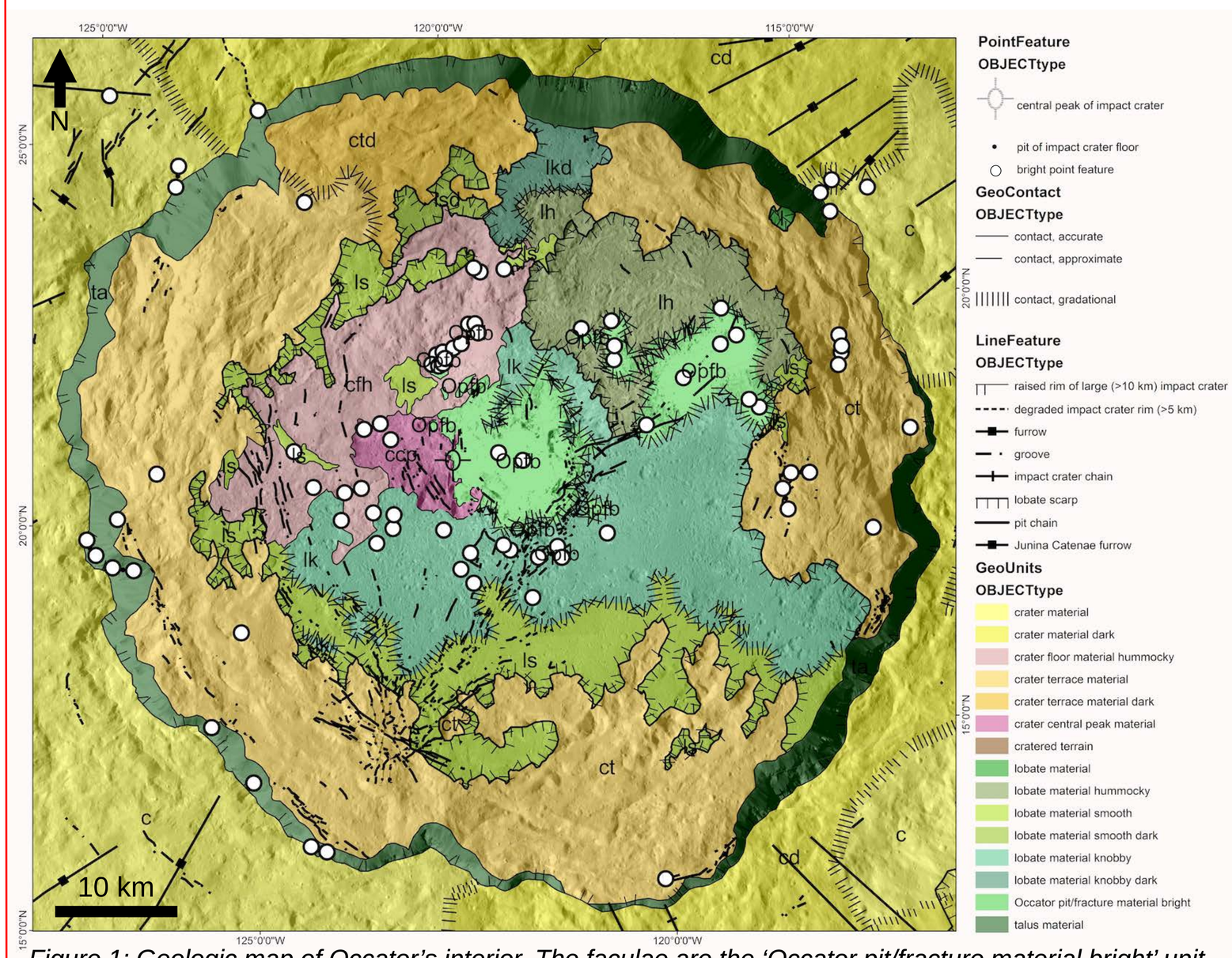

Figure 1: Geologic map of Occator's interior. The faculae are the 'Occator pit/fracture material bright' unit.

- INTERPRETATIONS & CONCLUSIONS -

Proposed geologic history:

1. The Occator-forming impactor hit part of Hanami Planum, a topographically high region with a negative Bouguer anomaly (Ermakov et al., 2017), which may be less devolatilized than other regions of Ceres (Raymond et al., 2017).
2. The impactor came at ~30-45° from the NW.
3. Shortly after the impact, crater-wall collapse and mass wasting formed terraces and hummocky crater floor materials.
4. The lobate materials were emplaced in the crater floor as impact melt, with possible enhanced mobility/volume due to impact-heated volatiles that were pre-existing in Hanami Planum (Bowling et al.; Schenk et al., Neesemann et al., 2017).
5. Volatile loss from the lobate materials forms the central pit with its bright Cerealia Facula coating (Schenk et al.; Stein et al., 2017; De Sanctis et al., 2016).
6. Inflation of a subsurface sill forms the hummocky lobate materials in the NW and factures throughout the crater (Buczkowski et al., 2017).
7. Some fractures are conduits used by the Vinalia-Faculae-forming materials to erupt onto the surface (Ruesch et al.; Buczkowski et al.; Nathues et al., 2017).
8. Final freezing of the lobate material forms a fractured dome within the Cerealia Facula (Buczkowski et al.; Schenk et al.; Nathues et al., 2017).
9. Small impactors expose even brighter, fresher material within Cerealia Facula, consistent with darkening of the faculae material over time by space weathering (Bu et al., 2017). Also, later mass wasting forms talus along the steep crater walls (~30°).

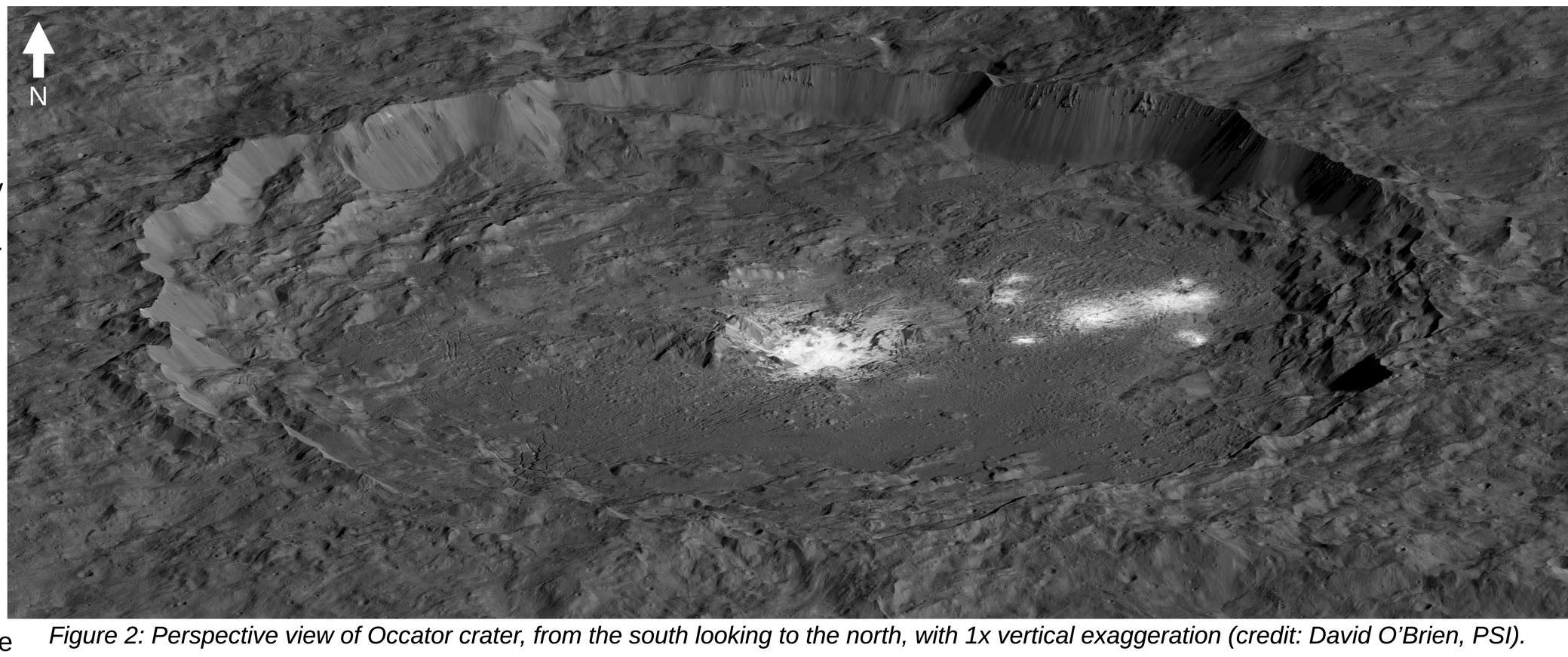

Figure 2: Perspective view of Occator crater, from the south looking to the north, with 1x vertical exaggeration (credit: David O'Brien, PSI).

National Aeronautics and Space Administration

Jet Propulsion Laboratory
California Institute of Technology
Pasadena, California

www.nasa.gov

Additional co-authors:
D. L. Buczkowski[2], P. M. Schenk[3], A. Neesemann[4], C. T. Russell[5], M. T. Bland[6], J. C. Castillo-Rogez[1], A. Ermakov[1], L. C. Quick[7], O. Ruesch[8], B. E. Schmidt[9], [1]Jet Propulsion Laboratory, California Institute of Technology, Pasadena, CA, USA, [2]JHU APL, Laurel, MD, USA, [3]LPI, Houston, TX, USA, [4]Free University of Berlin, Berlin, Germany, [5]UCLA, Los Angeles, CA, USA, [6]USGS, Astrogeology Science Center, Flagstaff, AZ, USA, [7]Smithsonian Institution, CEPS, Washington, DC, USA, [8]NASA GSFC, Greenbelt, MD, USA, [9]Georgia Institute of Technology, Atlanta, GA, USA.

Acknowledgements:
We thank the Dawn Flight Team at JPL for the development, cruise, orbital insertion and operations of the Dawn spacecraft. We thank the instrument teams at the Max Planck Institute, German Aerospace Center (DLR), Italian National Institute for Astrophysics (INAF) and Planetary Science Institute (PSI) for the acquisition and processing of Dawn data.

Poster No. P-04

Low Thermal Inertia Volcanic Deposits on the Moon

C. M. Elder[1] (3223)
P. O. Hayne[1] (3223) [1]Jet Propulsion Laboratory, California Institute of Technology

Introduction

- Volcanism is the surface expression of the thermochemical evolution of a planet.
- Studying lunar volcanism can help to answer questions such as *what is the bulk composition of the lunar mantle? What is the volatile content of the lunar mantle (at formation and now)? Is the lunar mantle still convecting today?*
- Lunar maria, the most prominent volcanic deposits on the Moon, formed between 4.0 and 1.2 Gyr ago with the majority forming between 3.8 and 3.3 Gyr ago [1].
- Recent high resolution imagery suggests that 'irregular mare patches' (IMPs) may be volcanic features that formed within the last 100 Myr [2].
- Modeling suggests that volcanism should not be possible this recently on the Moon [e.g. 3, 4].
- Here, we look at the thermal inertia of volcanic deposits to constrain their material properties.

Methods

- Fit Diviner nighttime measurements from [5]
- Temperatures exclude rocks >1 m
- The lunar near-subsurface is best fit by a model in which the thermal conductivity and density increase exponentially with depth, z: $\rho(z) = \rho_d - (\rho_d - \rho_s)\, e^{-z/H}$ where ρ_d is the density at depth and ρ_s is the density at the surface
- Solve for H
- Low H → high thermal inertia → more small rock fragments or a lower porosity

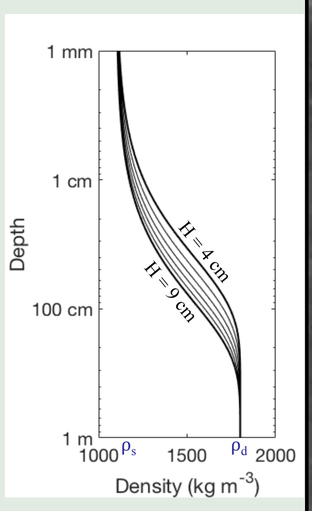

Summary of Results

(see timeline to the right for more details)

- Lunar red spots have a lower thermal inertia than the surrounding lunar regolith.
- Regional pyroclastic deposits have a lower thermal inertia than the surrounding regolith.
- Localized pyroclastic deposits do not show a thermal inertia anomaly.
- Ina has a low thermal inertia signature associated with its largest smooth mound.

Conclusions

- Lunar red spots are highly vesicular.
- Regional pyroclastic deposits are composed of small crystalline and/or glass beads.
- Multiple explanations could explain localized pyroclastic deposits.
- Ina includes either pyroclastic deposits or highly vesicular rocks.

National Aeronautics and Space Administration
Jet Propulsion Laboratory
California Institute of Technology
Pasadena, California

www.nasa.gov

Timeline of Volcanism on the Moon

Formation

4 Ga

3 Ga

Lunar maria formation

2 Ga

1 Ga

Present

Lunar Red Spots

- Previous work: Spectrally red, often embayed by mare basalts, many are domes with steep slopes, some are smooth plains or rugged patches of material, some have an evolved composition (highly silicic and thorium anomaly).
- Formation hypothesis: Viscous lava similar to terrestrial dacites, basaltic andesites, or rhyolites. Lava source is still debated; possibly basaltic underplating.
- Prediction: Steep slopes should be rocky, so they should have a high thermal inertia.
- Results: Lower thermal inertia than surrounding terrain.
- Implications: So porous that their density is lower than fine grained regolith → highly vesicular rock.
- Future work: Implications for lava source? Calculate volatile content necessary to produce observed density?

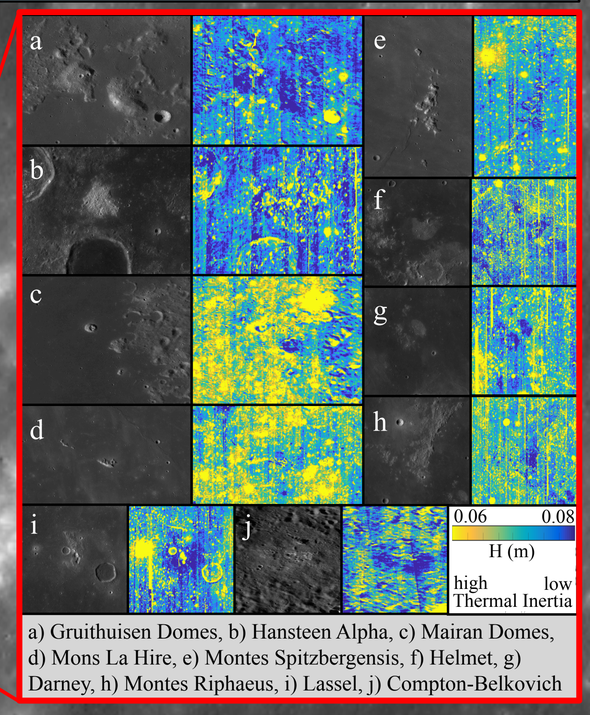

a) Gruithuisen Domes, b) Hansteen Alpha, c) Mairan Domes, d) Mons La Hire, e) Montes Spitzbergensis, f) Helmet, g) Darney, h) Montes Riphaeus, i) Lassel, j) Compton-Belkovich

Majority of lunar maria formation

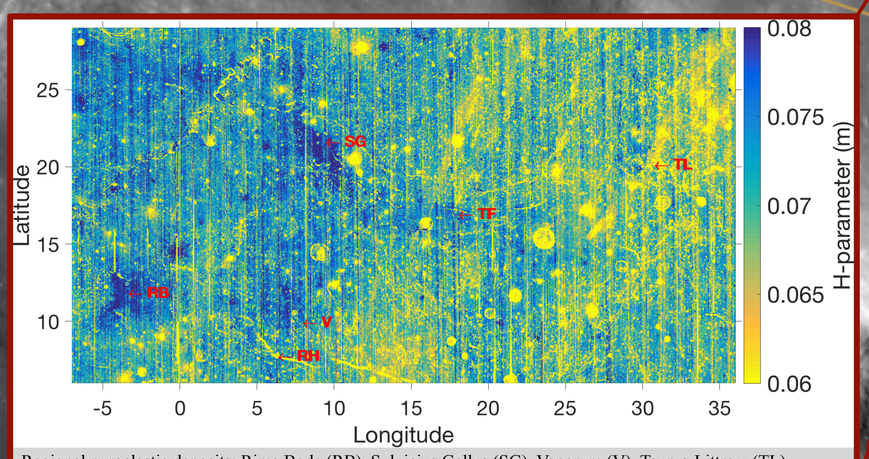

Regional pyroclastic deposits: Rima Bode (RB), Sulpicius Gallus (SG), Vaporum (V), Taurus-Littrow (TL), Tacquet Formation (TF), Rima Hyginus (RH)

Regional Pyroclastic Deposits

- Previous work: Low-albedo units composed of small crystalline and/or glass beads; larger than 2,500 km^2.
- Formation hypothesis: Lava-fountain eruptions.
- Prediction: Lower thermal inertia than surrounding regolith, which has more small rock fragments and less glass.
- Results: Lower thermal inertia than surroundings to varying degrees.
- Implications: They are composed of small crystalline and/or glass beads, but variation between deposits requires further work.

Alphonsus NE

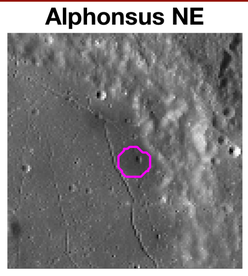

A localized pyroclastic deposit in the north east portion of Alphonsus crater. It may have a thermal inertia value slightly lower than its surroundings, but the histograms of H values on and off the deposit show only a slight increase in H (decrease in thermal inertia) for the pyroclastic deposit.

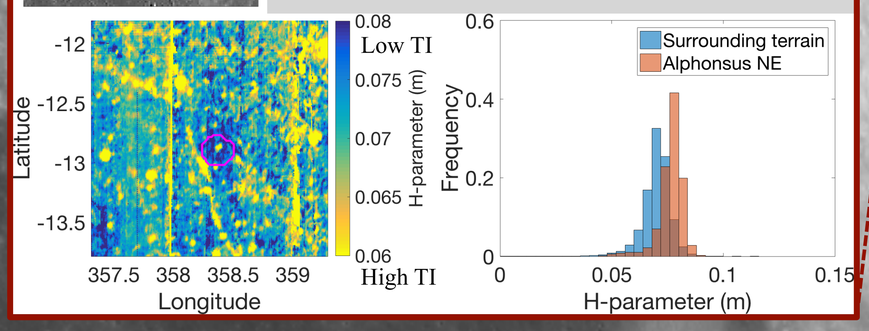

Localized Pyroclastic Deposits

- Previous work: Low-albedo units composed of small crystalline and/or glass beads but may also include country rock; smaller than 2,500 km^2.
- Formation hypothesis: Vulcanian-style eruptions.
- Prediction: Small beads would have a low thermal inertia, but country rock could increase the overall thermal inertia of the deposit.
- Results: Typically no thermal inertia anomalies.
- Implications: Multiple possible explanations: 1) Small (in area), so easily covered by rocks ejected by nearby impacts; 2) Thin, so easily punctured by impacts; and/or 3) Original eruption incorporated a significant amount of country rock.

Irregular Mare Patches

- Previous work: Uneven terrain interspersed by smooth mounds; maximum dimension ranges from 100-5000 m; 70 have been discovered; crater counts, spectral properties, topographic relief and surface texture all suggest they are young (but this contradicts our understanding of the thermal evolution of the Moon).
- Formation hypothesis: Very controversial. Possibilities include: caldera collapse, explosive outgassing, lava flow inflation, pyroclastic eruption, regolith drainage into sub-surface voids, or magmatic foams.
- Prediction: Depends on hypothesis.
- Results: Ina has a low thermal inertia, with the lowest values concentrated on largest smooth mound.
- Implications: Pyroclastic deposits or porous solidified magmatic foam could explain the low thermal inertia anomaly at Ina. If pyroclastic, consistent with young age.

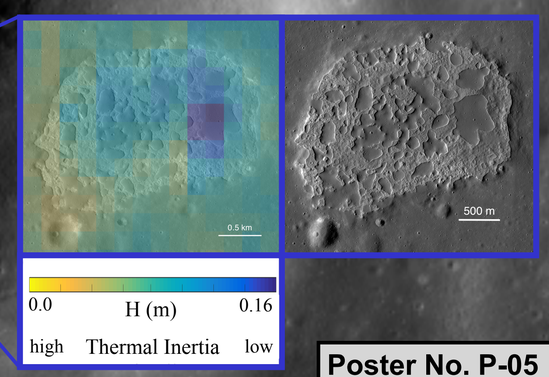

References: [1] Hiesinger et al. (2011) *GSA Spec. Pap.*, 477, 1-51. [2] Braden et al. (2014) *Nat. Geosci.* 7 (11), 787-791. [3] Ziethe et al. (2009) *Planet. Space Sci.* 57 (7), 784-796. [4] Solomon and Head (1980) *Rev. Geophys.* 18 (1), 107-141. [5] Bandfield et al. (2011) *J. Geophys. Res.* 116 (E12).

Poster No. P-05

National Aeronautics and Space Administration

A Search for Temporal Changes on Pluto and Charon

Jason D. Hofgartner (JPL Section 3224), Bonnie J. Buratti (3224), Spencer L. Devins (3224), R. A. Beyer[1], P. Schenk[2], S. A. Stern[3], H. A. Weaver[4], C. B. Olkin[3], A. Cheng[4], K. Ennico[1], T. R. Lauer[5], J. Spencer[3], L. A. Young[3], and the New Horizons Science Team

1. NASA Ames Research Center, Moffett Field, CA; 2. Lunar and Planetary Institute, Houston, TX; 3. Southwest Research Institute, Boulder, CO; 4. Johns Hopkins University Applied Physics Laboratory, Laurel, MD; 5. National Optical Astronomy Observatory, Tucson, AZ;

1. Summary

The discovery of young surfaces in the Pluto system that imply ongoing geologic activity motivated a search for temporal changes on Pluto and Charon. A thorough search for temporal changes using New Horizons images was completed. Images that covered the same region were blinked and manually inspected for any differences in appearance. Changes of appearance between different images were observed but in all cases were attributed to variability of the imaging parameters (especially geometry) or artifacts. No differences of appearance that are strongly indicative of a temporal change were found on the surface or in the atmosphere of either Pluto or Charon. Limits on temporal changes as a function of spatial scale and temporal interval during the New Horizons encounter are determined. Contrast reversal and high-phase bright features that change in appearance with solar phase angle are identified. The change of appearance of these features is most likely due to the change in phase angle rather than a temporal change. Had active plumes analogous to the plumes discovered on Triton by Voyager 2 been present on the encounter hemispheres of either Pluto or Charon, they would have been detected. Several dark streak features that may be deposits from past plumes are identified.

2. Motivation: Young Surfaces

Temporal changes are generally more likely to be observed between images with longer time intervals. Due to the flyby architecture of the New Horizons mission, the period of geologically resolved imaging was relatively short, a consideration that decreases the probability that temporal changes were detected. Nonetheless, there were three reasons for conducting a search for temporal changes:

1. Pluto and Charon have young surfaces and features that imply ongoing or recent geologic activity (Stern et al., 2015),
2. Temporal changes of plumes on Triton were observed in images with similar temporal intervals and spatial resolutions (Soderblom et al., 1990),
3. The significant scientific rewards from detection of temporal changes outweighed the concern of lower return on investment in the event that no temporal changes were detected.

3. Methodology: Manual Inspection

To search for temporal changes, images of the same region were blinked and manually inspected for any differences of appearance. Two researchers checked each image pair. An automated change detection algorithm is conceivable but manual inspection of the image pairs was favored because the imaging geometry varied drastically between some images and the phase space of conceivable changes in appearance is broad.

The search for temporal changes on Pluto and Charon was divided into three parts for each body:

1. Full-disk Long Range Reconnaissance Imager (LORRI) images/mosaics such that all regions were investigated (except the part of the southern hemisphere in winter darkness),
2. Higher resolution LORRI image mosaics of parts of the encounter hemispheres,
3. Multispectral Visible Imaging Camera (MVIC) images with information about temporal variability not encompassed by parts 1 and 2.

4. Conclusions: No Temporal Variability

1. No changes in appearance that are strongly indicative of a temporal change were found on the surface or in the atmosphere of either Pluto or Charon.
2. On Pluto's encounter hemisphere, there were no temporal changes > 1 km in scale over ~3 hour period, > 2 km over ~7 hours, and > 40 km over one rotation period (~6.4 Earth days). On Pluto's non-encounter hemisphere, there were no temporal changes > 63 km in scale over one rotation period. For ~5% of Pluto's surface, there were no temporal changes > 400 m in scale over ~1 hour period. On Charon's encounter hemisphere, there were no temporal changes > 1.5 km in scale over ~5 hour period and > 40 km over one rotation period. On Charon's non-encounter hemisphere, there were no temporal changes > 35 km in scale over ~3/8 of a rotation period. For ~23%, of Charon's surface, there were no temporal changes > 700 m, over ~2.5 hour period.
3. Had active plumes analogous to the plumes discovered on Triton by Voyager 2 been present on the encounter hemispheres of either Pluto or Charon, they would have been detected.

5. Interesting Example #1: Contrast Reversal Features on Pluto

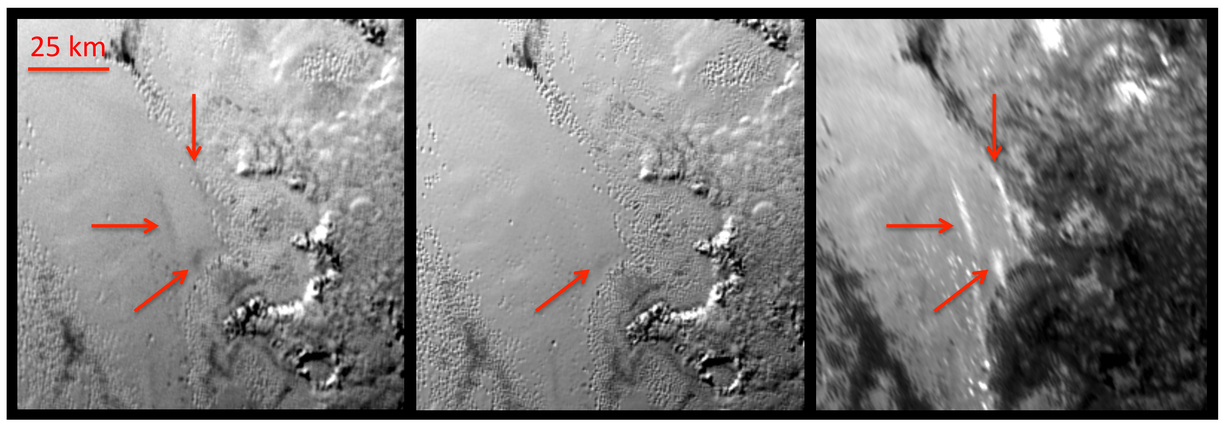

The areas indicated with red arrows change in appearance between these three images of part of Pluto's Sputnik Planitia. They are contrast reversal features that are dark relative to their surrounding terrain at low solar phase angle (25^{O}, left panel), not/barely apparent at intermediate phase (47^{O}, middle panel), and brighter than their surroundings at high phase (151^{O}, right panel). The change of appearance is due to the change of solar phase angle rather than a temporal change on Pluto. The darkening of regions at the right and bottom left of the right panel is also due to the high phase angle, most likely shadowing, and the bright features at the top right are additional examples of contrast reversal features.

6. Interesting Example #2: High-phase Bright Features on Pluto

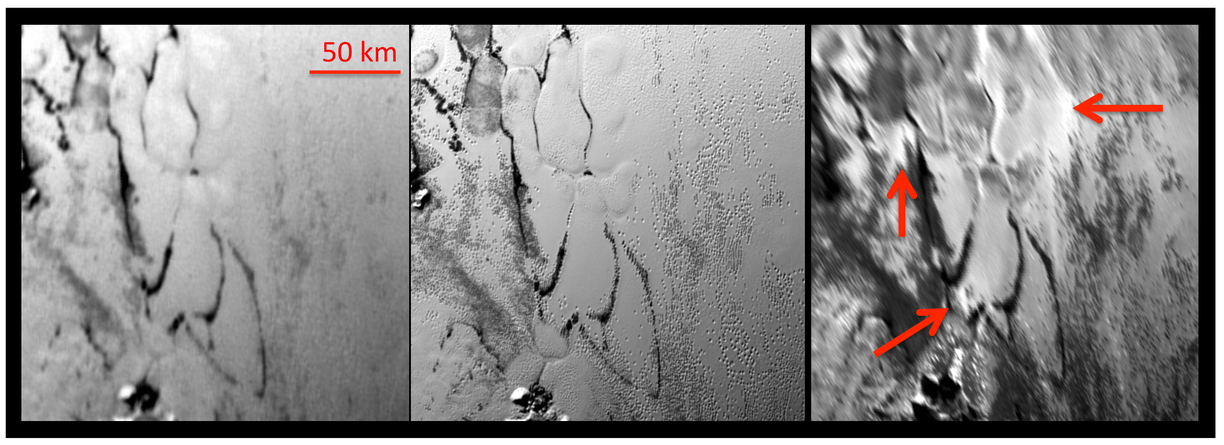

The red arrows indicate some areas of Pluto's Sputnik Planitia that change in appearance between the right panel and the other two panels. Bright features are observed at high solar phase angle (151^{O}, right panel) but not in any lower phase angle images (19^{O}, left panel; 69^{O}, middle panel; 25^{O}, 38^{O}, and 47^{O}, not shown). Other areas in these images also exhibit the same behavior. The change of appearance is due to the change of phase angle rather than a temporal change on Pluto. The darkening of many areas in the right panel is also due to the high phase angle, most likely shadowing.

7. Dark Streaks on Pluto: Possible Plume Deposits

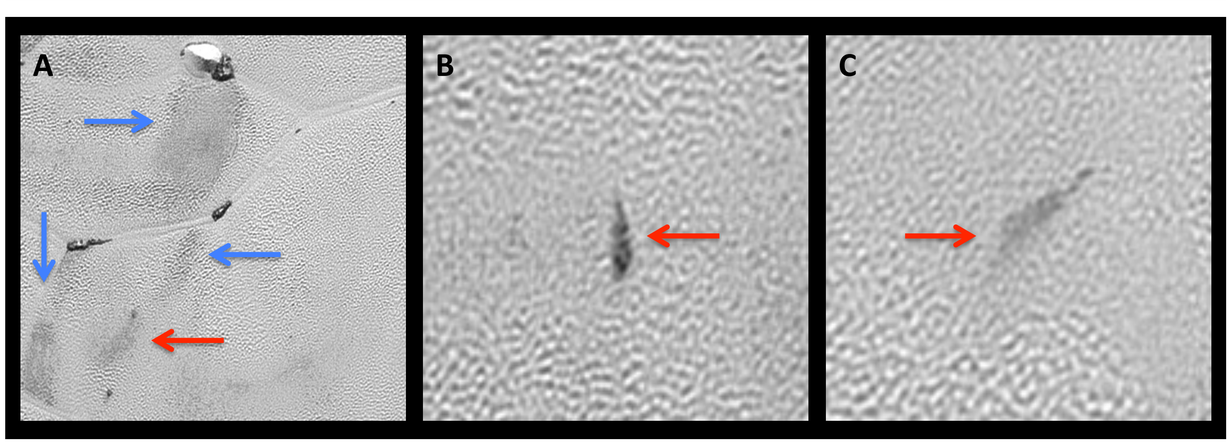

A few examples of dark surface streaks on Pluto. Blue arrows in panel A indicate streaks in Sputnik Planitia that are adjacent to hills and may be the result of interactions between the hills and winds (Stern et al., 2015). Red arrows in panels A-D indicate a few streaks in Sputnik Planitia that may be smaller examples of the streaks indicated by blue arrows in panel A or that may be the result of previous plumes such as those observed on Triton (Soderblom et al., 1990). Panel A is ~70 km by 70 km and panels B and C are ~16 km by 16 km.

National Aeronautics and Space Administration

Jet Propulsion Laboratory
California Institute of Technology
Pasadena, California

www.nasa.gov

Acknowledgements: Jason Hofgartner gratefully acknowledges the entire New Horizons team for the incredible exploration of the Pluto system that enabled this research. Jason Hofgartner was supported by an appointment to the NASA Postdoctoral Program at the NASA Jet Propulsion Laboratory, California Institute of Technology administered by Universities Space Research Association through a contract with NASA. This research has made use of the USGS Integrated Software for Imagers and Spectrometers (ISIS).

Poster No. P-06

National Aeronautics and Space Administration

Spectral Behavior of Irradiated Sodium Chloride Crystals Under Europa-Like Conditions

Michael J Poston (3225)
Kevin Hand (3204), Robert Carlson (3227)

Motivation: Ocean World Habitability

Key Question:
Is there exchange between the ocean and the surface?

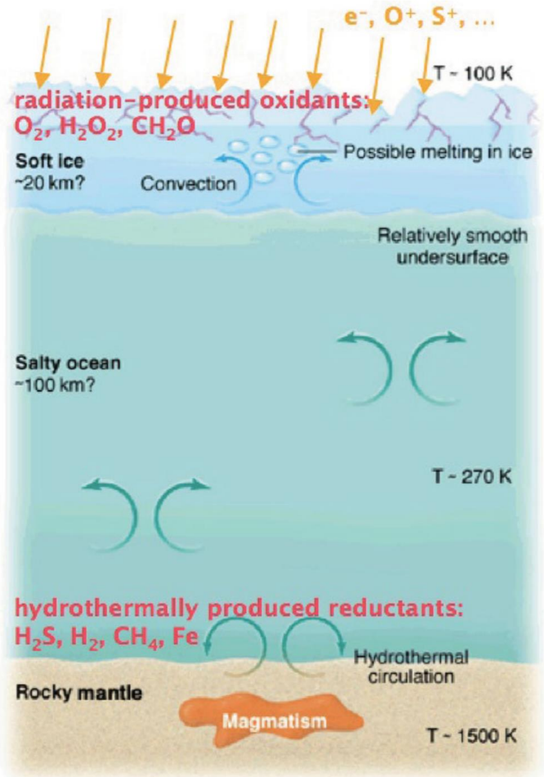

Figure 9. Representation of Europa's ice shell, ocean, and rocky mantle (after Stevenson, 2000). Oxidants are produced at Europa's surface by ion irradiation (arrows). Reductants might be produced at the ocean floor if the mantle rock is hot, promoting hydrothermal circulation. Such oxidants and reductants could serve to fuel life in Europa's ocean.

Exchange likely creates chemical disequilibrium. Life (as we know it) thrives on chemical disequilibrium.

Approach:
NaCl as a tracer of an Earth-like ocean

Hand and Carlson 2015

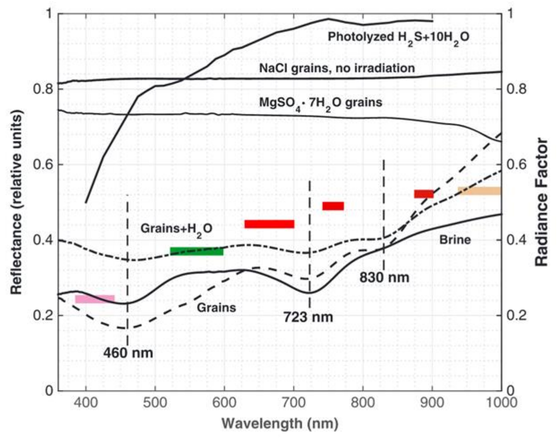

NaCl irradiation in Europa-like conditions forms lattice defects called "color centers"

Identifying such color centers on an ocean world would indicate an exposure of NaCl, likely from the ocean

Fischer, Brown, and Hand (2015); Fischer et al. (2017); Ligier et al. (2016); have detected a surface component interpreted as chloride salts of endogenic origin.

- Are any of these areas geologically-young?

Roth et al. (2015); Sparks et al. (2016); have detected possible plumes of material over localized regions of Europa

- Are these plumes (if real) bringing up material from the ocean?

Science Question

Can the dynamics of color center formation in NaCl be used to trace the surface exposure age of an NaCl deposit on the surface of Europa?

Approach

Perform a sequence of experiments in the Minos ultra-high vacuum chamber in the Icy and Ocean Worlds Simulation Laboratory while tracking color center formation

Temperature (K)	e- Flux (nA, 10keV)	Duration (hours)	Fluence (eV / 16 amu)	Europa Equivalent (yrs)
100	250	116.2	670	67
100	--	27.8	--	--
130	--	53.2	--	--
150	--	18.0	--	--
170	--	25.8	--	--
190	--	24.2	--	--
200	--	22.9	--	--
230	--	48.8	--	--
260	--	47.0	--	--
290	--	95.3	--	--
290	250	52.0	300	30
290	--	89.0	--	--
cooling	--	2.5	--	--
180	250	50.9	290	29
180	--	69.0	--	--
cooling	--	2.2	--	--
100	57	47.3	62	6
100	125	1.7	5	1
power failure*	--	18.2	--	--
cooling	--	3.0	--	--
100	125	52.8	150	15
100	--	119.1	--	--

This sequence included irradiation at:

- Three different fluxes (at constant temperature)
- Three different temperatures (at constant flux)

Relaxation (decay of color centers) at:

- A sequence of increasing temperatures
- Three fixed temperatures

*Power failed briefly, shutting down the pumps and all electronics except the cryostat. Sample was exposed to about 300 torr of air for a few minutes before vacuum was restored. Sample was subsequently held at 200K overnight before proceeding.

Application to JPL

Europa Clipper – Finding the youngest features is helpful for habitability goals
– Aids in confirmation of locations of plume fallout
Europa Lander – Finding the youngest deposits for landing site selection enhances the science return for habitability and life detection goals

References

Fischer et al. (2015) doi:10.1088/0004-6256/150/5/164
Fischer et al. (2017) doi:10.3847/1538-3881/153/1/13
Hand and Carlson (2015) doi:10.1002/2015GL063559
Ligier et al. (2016) doi:10.3847/0004-6256/151/6/
Roth et al. (2015) doi: 10.1126/science.1247051
Sparks et al. (2016) doi:10.3847/0004-637X/829/2/12

Results

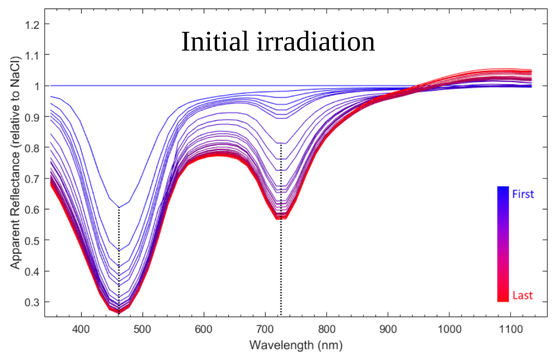

(left) – initial irradiation – 10keV electrons at 250nA at 100K
- Features form at 460nm and 720nm

(both) The first six spectra are 15 minutes apart and following spectra are about 2.5 hours apart

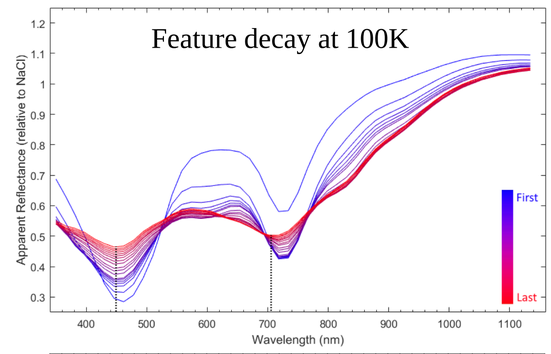

(right) – feature decay at 100K
- Primary features decreased in band depth and shifted to shorter wavelengths.
- Minor features appeared at about 600nm, 820nm, and 910nm

(right) – feature decay with increasing temperature
- Last spectrum from each hold temperature during the extended decay sequence
- By the end:
  - 460nm band had all but disappeared
  - 720nm band had shifted to about 670nm and decayed substantially
- Small additional features appear to have formed at about 360nm and 520nm and remained at 290K

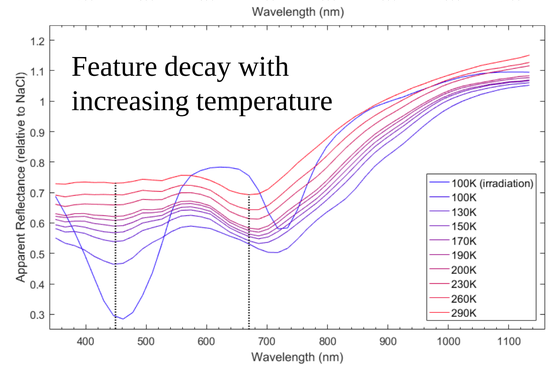

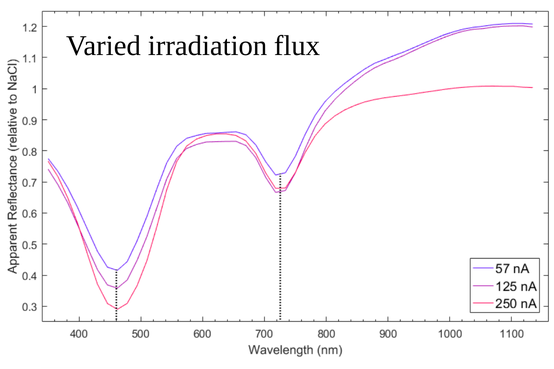

(top left) – varied irradiation flux – similar dose at 100K
- Lesser flux resulted in slightly shallower bands

(lower left) – varied temperature flux – similar dose at 250nA
- Lower temperature resulted in deeper bands

(lower right) – decay at fixed temperatures – equal duration
- Faster decay at higher temperature

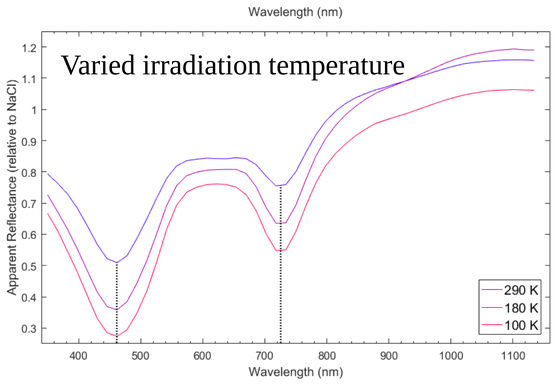

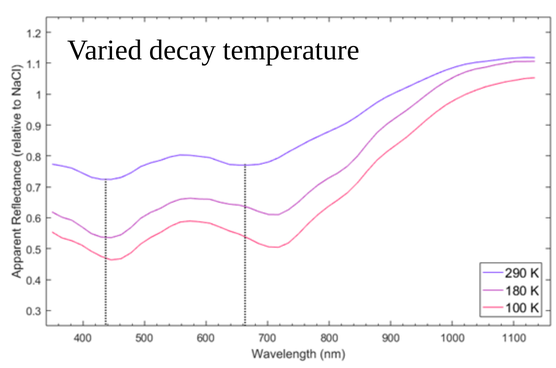

Analysis

(right) – continuum-removed band depths for symmetric peaks for:
(top right) – continuum-removed band depth for symmetric peak centered at 718 nm
(middle) – peak centered at 462nm
(bottom) – ratio of 718/462nm band depths
- The band depth ratio produced the most consistent results from irradiation to irradiation.

(lower left) – curve fit of band depth ratio (y) as a function of dose (x)
(lower right) – relative error of curve fit
- First irradiation was used as most representative of fresh NaCl exposure
- Valid to 200 eV/amu
- Invert to obtain:

$$x = \exp\left(\frac{y + 0.16}{0.12}\right) + 0.0014$$

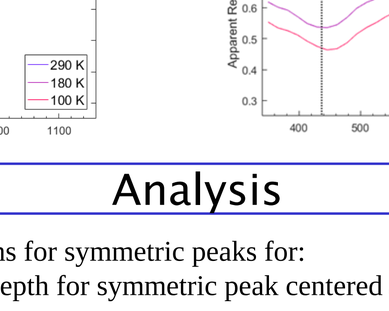

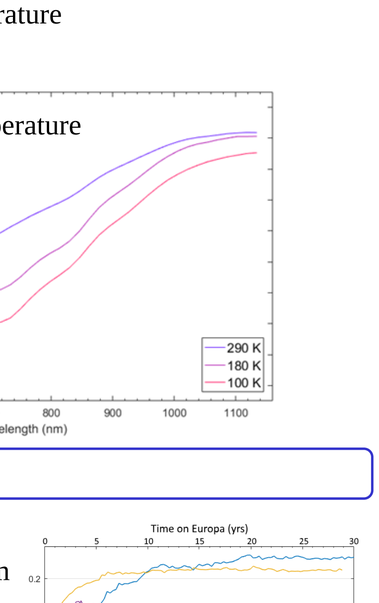

Conclusions

- ✓ Presence of color center defects under irradiation is a dynamic equilibrium of creation and thermal loss
- ✓ Color centers at 460 and 720 nm are created at different rates under different conditions
- ✓ Ratio of 720/460 band depth is largely independent of irradiation conditions
- ✓ 720/460 ratio can be used to trace the surface exposure age of NaCl deposits in irradiation environments
  - Requires knowledge of the dose rate at the feature location

Poster No. P-07

National Aeronautics and Space Administration

Laboratory simulation of hot exoplanetary atmospheres

Benjamin Fleury (3227)
Murthy Gudipati (3227), Bryana Henderson (3227), Demian Marchione (3227)

Introduction

With new missions such as TESS and JWST on the horizon, challenges are mounting to determine the contributions of aerosols to chemical and radiative coupling in exoatmospheres. The aim of our work is to undertake laboratory simulations to help determine the equilibrium atmospheric chemical composition and aerosol formation efficiencies of exoplanets whose observable atmospheric temperatures vary between 300 K and 1800K, a range that covers relatively cool terrestrial exoplanets to hot-Jupiter-like exoplanets. In this work, we have studied thermal chemistry in exoplanet atmospheres by conducting experiments with H_2/CO gas mixtures to simulate a hydrogen-dominated atmosphere with a C/O ratio of 1.

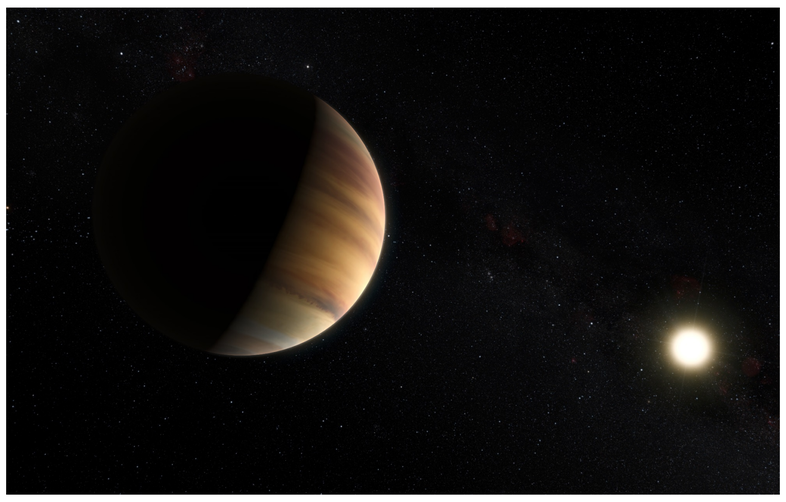

Artistic view of 51 Pegasi B, a Hot-Jupiter like exoplanet. These exoplanets orbit closely to their stars. Their atmospheres experience high temperature and high UV radiation conditions.
New experimental research is critical to understand photochemistry and aerosols formation in these unexplored environments.

Credit:ESO/M. Kornmesser/Nick Risinger (skysurvey.org)

High temperature cell built at JPL

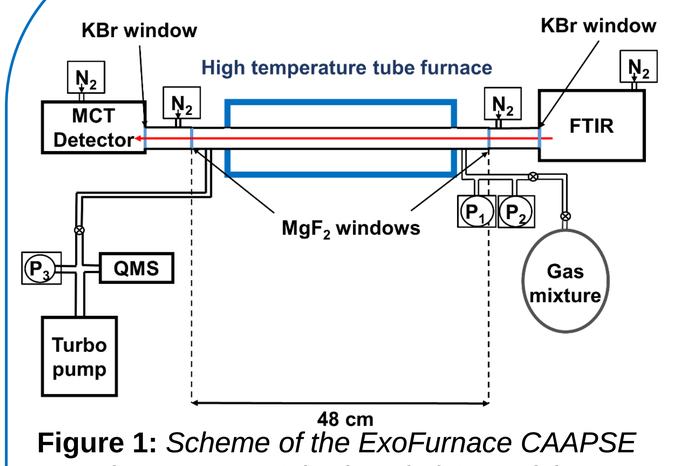

Figure 1: *Scheme of the ExoFurnace CAAPSE experiment concept (top) and picture of the CAAPSE in action at 1773 K at JPL (bottom).*

To study this chemistry we used the CAAPSE experiment ("high-temperature Cell to simulate Atmospheric and Aerosol Photochemistry and Spectroscopy of Exoplanets), recently built at JPL and presented in Figure 1. The cell is filled with 15 mbar of a H_2:CO mixture with a mixing ratio of 5:1 and then warmed up to the studied temperatures. The evolution of the gaseous phase composition is monitored using infrared spectroscopy to determine the thermal equilibrium composition.

IR monitoring of the gas phase composition

The evolution of the gaseous phase composition is monitored using IR spectroscopy in the 1800-3200 cm^{-1} range.

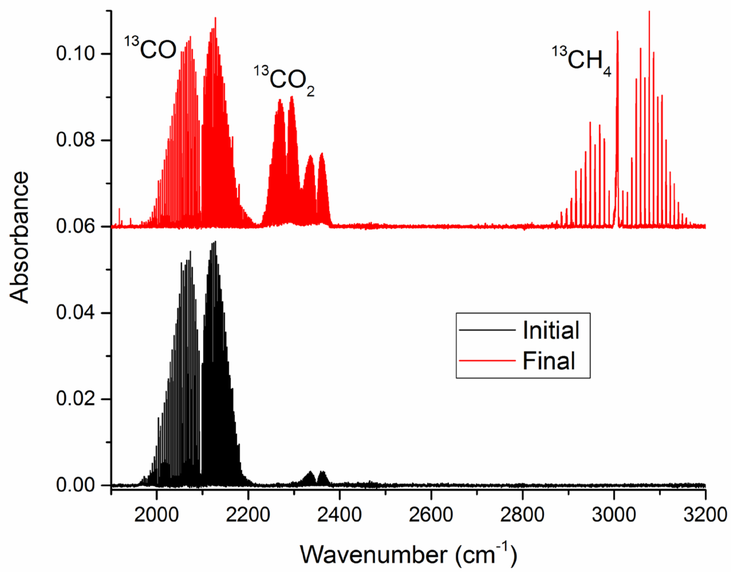

Figure 2: *Evolution of the gaseous phase composition with a H_2:CO mixture before the experiment (black) and at the thermal equilibrium (red) when heated at 1173 K in an alumina cell.*

Figure 2 shows a modification of the gaseous phase composition at the thermal equilibrium relative to the initial composition with:

- A decrease of the ^{13}CO absorption band (2096 cm^{-1}).
- The detection of 2 new absorption bands attributed to: $^{13}CO_2$ (2283 cm^{-1}) and $^{13}CH_4$ (3009 cm^{-1}).

This demonstrates that thermal chemistry can occur in H_2:CO dominated atmospheres at high temperature, impacting the equilibrium chemical composition.

Catalytic effect of the alumina on the CH_4 formation

Wall reactions can impact the chemistry simulated in laboratory experiments. To evaluate this phenomenon, we repeated the experiment using a quartz high temperature cell instead of the alumina reaction cell used before.

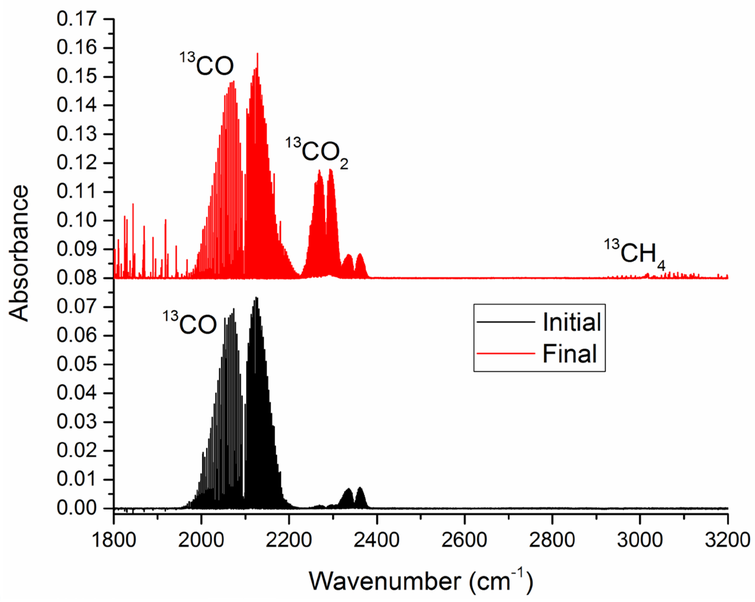

The Figure 3 shows quantitative differences when the experiment is realized with the quartz cell. The formation of $^{13}CO_2$ and $^{13}CH_4$ is less important than for the experiment realized with the alumina cell.
These results point out that thermal chemistry could be catalyzed by surface reactions on the alumina tube.

Figure 3: *Evolution of the gaseous phase composition with a H_2:CO mixture before the experiment (black) and at the thermal equilibrium (red) when heated at 1173 K in a quartz cell.*

Conclusion and perspectives

We realized a first experimental study of the thermal chemistry in a H_2:CO dominated atmosphere. We observed the formation of CO_2 and CH_4. Methane production is enhanced by several orders of magnitude when reactions are catalyzed by the alumina compositing the reaction cell.

Further studies will be realized to:

- Quantify the different species detected at the thermal equilibrium and the evolution of the TEC with the temperature.
- Determine the importance of the catalytic effect of silicate grains on the reactivity of hot exoplanets atmosphere
- Simulate the photochemistry in hot exoplanet atmospheres by simultaneously irradiating and heating the gas mixture.

National Aeronautics and Space Administration
Jet Propulsion Laboratory
California Institute of Technology
Pasadena, California

www.nasa.gov

Acknowledgments

This research work has been supported by the Strategic R&TD funding under "Exoplanet Science Initiative, ESI". We thank Dr. Mark Swain and Dr. Robert West for helpful discussions.

Poster No. P-08

National Aeronautics and Space Administration

International Space Station-Microbial observatory of pathogenic viruses, bacteria and fungi and the impact on astronaut health

Camilla Urbaniak (352N)

Crystal Jaing (LLNL), Satish Mehta (JSC), David Smith (ARC), Fathi Karouia (ARC) , Kasthuri Venkateswaran (352N)

Background

- Microbes are EVERYWHERE: They are found all over and inside your body, in the space craft assembly facility at JPL and in the harsh conditions of Earth and space
- This collection of microbes in a given environment is called the "microbiome"
- There are more microbes in our body than human cells and there are more microbes in a teaspoon of soil than there are people in the world
- Various types of bacteria are found in a given environment:

Commensals: Generally considered "friendly' or "good" bacteria, that have positive benefits for the host

Opportunistic pathogens: These microbes can cause problems if the host is not as "healthy" such as in individuals who are immune-compromised

Pathogens: Cause disease in a wide variety of hosts, regardless of health status.

- Studies on Earth have shown that changes in certain factors can alter the balance of these different types of microbes BUT data is limited on how space conditions change this composition and the impact of these changes to the biological and inert objects in that environment.

Study Goals

How does space flight change the composition and function of the human microbiome

-How long do these changes last

-What is the impact on astronaut health- during missions and long term

Is there a change in the relative proportions of pathogens

-What are the anti-microbial resistance and virulence genes found in these pathogens

-Is there an increased rate of transfer of these "bad" genes while astronauts are in space

Does space flight induce re-activation of latent viruses

-Is there a microbiome signature that is correlated with viral load from latent viruses

What viral, fungal and bacterial pathogens are found on surfaces and in the air of the ISS

-Are there certain microbes found at certain locations

-How does humidity, temperature, occupant density etc shape the ISS microbiome

-Are there certain locations that have a higher amount of microbes that form biofilms

-How long do human associated microbes persist on surfaces

Is there transfer of pathogens or opportunistic pathogens between astronaut-surface-astronaut

Analyses:

- Microbiome (types of microbes)
- Metagenome (function of microbes)
- Transcriptome (function)
- Lawrence Livermore Microbial Detection Array
- Culture analysis
- Microbial load

Sample collection

Human samples

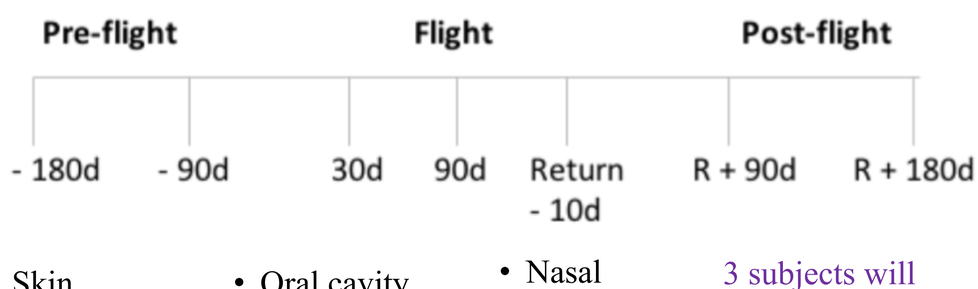

- Saliva
- Skin
  - Forehead
  - Forearms
  - Underarms
  - Naval
- Oral cavity
  - Cheeks
  - Gums
- Nasal cavity

3 subjects will be sampled over a span of 1.5 years

International Space Station

Surfaces and air: 8 different locations, sampled during 3 different flight missions, over a span of a year

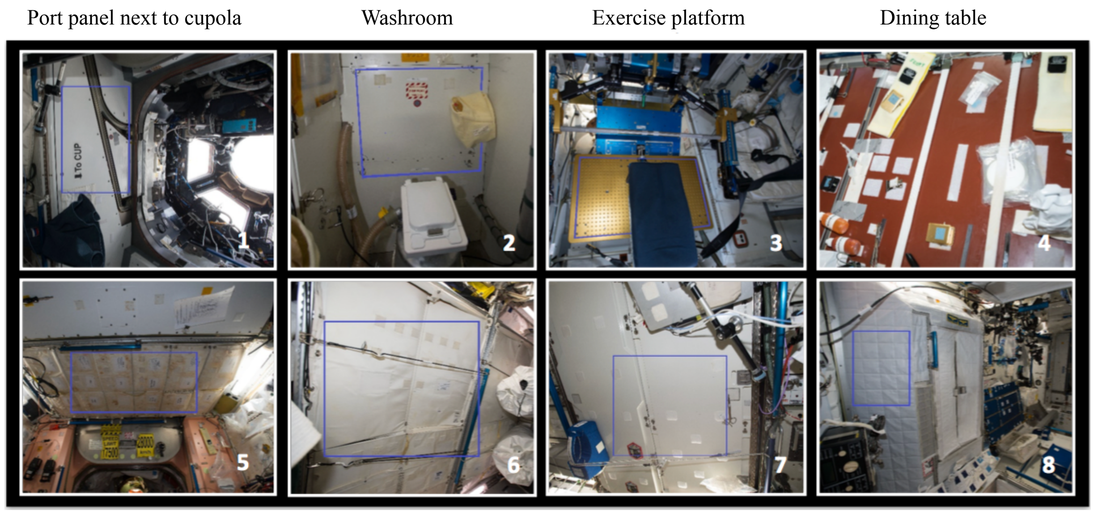

ISS surface wipe

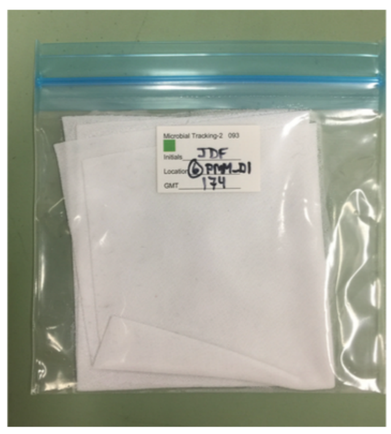

ISS air filter

Culture analysis

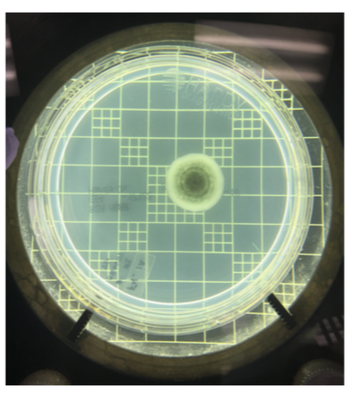

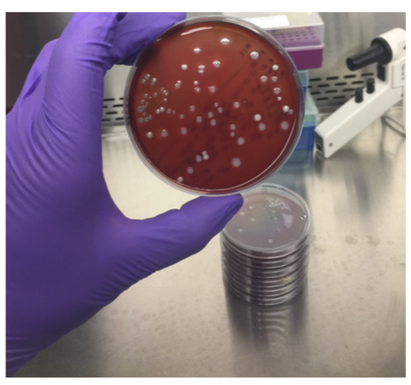

National Aeronautics and Space Administration

Jet Propulsion Laboratory
California Institute of Technology
Pasadena, California

www.nasa.gov

Poster No P-12.